

# Automatic generation of quarkonium amplitudes in NRQCD

---

**Pierre Artoisenet, Fabio Maltoni**

*Centre for Particle Physics and Phenomenology (CP3)*

*Université Catholique de Louvain*

*Chemin du Cyclotron 2, B-1348 Louvain-la-Neuve, Belgium*

*E-mails: pierre.artoisenet@uclouvain.be, fabio.maltoni@uclouvain.be*

**Tim Stelzer**

*Department of Physics, University of Illinois at Urbana-Champaign,*

*1110 West Green Street, Urbana, IL 61801*

*E-mail: tstelzer@uiuc.edu*

**ABSTRACT:** We present a simple method to automatically evaluate arbitrary tree-level amplitudes involving the production or decay of a heavy quark pair  $Q\bar{Q}$  in a generic  $^{2S+1}L_J^{[1,8]}$  state, i.e., the short distance coefficients appearing in the NRQCD factorization formalism. Our approach is based on extracting the relevant contributions from the open heavy quark-antiquark amplitudes through an expansion with respect to the quark-antiquark relative momentum and the application of suitable color and spin projectors. To illustrate the capabilities of the method and its implementation in MadGraph a few applications to quarkonium collider phenomenology are presented.

---

## Contents

<b>1. Introduction</b>	<b>1</b>
<b>2. Quarkonium amplitudes in NRQCD</b>	<b>3</b>
2.1 Projection method and its implementation	4
2.2 Relativistic correction to $S$ -wave state production	5
2.3 Polarization of vector-like quarkonium states	6
2.4 Validation and examples	7
2.4.1 Preliminary checks	7
2.4.2 Example 1: $B_c$ production at various colliders	8
2.4.3 Example 2: Higgs decay into $\Upsilon + X$ .	9
<b>3. Applications</b>	<b>10</b>
3.1 $\gamma\gamma \rightarrow J/\psi + X$ at LEP II	10
3.2 $e^+e^- \rightarrow \eta_c + X$ at $\sqrt{s} = 10.6$ GeV	11
3.3 $p\bar{p} \rightarrow \Upsilon + X$ at the Tevatron	13
<b>4. Conclusions and Outlook</b>	<b>14</b>

---

## 1. Introduction

Bound states of heavy quarks, such as  $J/\psi$ ,  $\Upsilon$  or  $B_c$ , are unique systems where our understanding of QCD both at the perturbative and non-perturbative level can be tested. Since the mid seventies, when  $J/\psi$  was discovered and asymptotic freedom invoked to explain its narrow width, an impressive amount of experimental data have provided continuous challenges to the theoretical community. To date several open questions remain to be answered that concern both production and decay mechanisms [1].

One of the outstanding issues is to what extent a non-relativistic treatment of a quarkonium system is a useful starting point to describe the production and decay of bound states of heavy quarks. This is best tested in the case of charmonium, where the mass is not too far from  $\Lambda_{QCD}$ . The appeal of such an approach, is the possibility of embedding it in a rigorous framework, non-relativistic QCD (NRQCD) [2], that allows one to make consistent theoretical predictions which can systematically be improved. NRQCD is an effective field theory that can be matched to full QCD. Effects of order  $Q^2 \geq m_Q^2$  are encoded in short distance coefficients that can be estimated by using perturbation theory. Low  $Q^2 < m_Q^2$  effects, typically those involving hadronization, are factorized into long-distance matrix elements, which are universal, can be organized hierarchically in powers of  $v$  and can be either measured on lattice simulations or extracted from experimental data.

Despite its theoretical appeal and undeniable successes, not all of the predictions of the NRQCD factorization approach have been firmly established. Consider for example the color-octet contributions in the  $J/\psi$  production: they seem to play a dominant role at the Tevatron and in  $\gamma\gamma$  collisions, but they look marginal at  $e^+e^-$  at low energy, in photoproduction at HERA [3] and in fixed-target experiments [4]. Another example is the of  $J/\psi$ 's at high- $p_T$  at the Tevatron. NRQCD predicts a sizeable transverse polarization in contrast to the latest data that now clearly indicate that  $J/\psi$ 's are not transversely polarized [5].

Given such a puzzling scenario, it is mandatory to re-examine in details the key observables and the corresponding available theoretical predictions and try to systematically improve on them. Two main directions can be followed.

The first is to calculate predictions for cross sections and relevant distributions at the next-to-leading order (NLO) accuracy in the strong coupling expansion. Even for a small number of final state partons these calculations are technically very challenging and only a few are currently available. For example, there are only three calculations relevant for describing the  $p_T$  of the quarkonium state at NLO at colliders, i.e., those whose born process is a  $2 \rightarrow 2$ : the  $\gamma\gamma \rightarrow {}^3S_1^{[1]} + \gamma + X$  [6], the pioneering  $\gamma p \rightarrow {}^3S_1^{[1]} + X$  [7] and the recently evaluated  $pp \rightarrow {}^3S_1^{[1]} + X$  [8]. In  $e^+e^-$  collisions the cross section to produce  ${}^3S_1^{[1]} c\bar{c}$  is the only inclusive charmonium cross section known at NLO [9].

The second way is to extend the set of the typical observables analyzed by studying new processes and also predicting more exclusive observables. To this aim, we propose to use a multi-purpose matrix element based generator. This kind of codes, which have become widely available recently, have dramatically reduced the burden of performing phenomenological studies at colliders. They automatically create the matrix elements corresponding to a given process and then generate unweighted parton-level events that can be passed to standard Monte Carlo programs such as Pythia [10] or Herwig [11], for showering and hadronization, and eventually to detector simulation. The advantages of such an approach are numerous. The most important one is that any theoretical description (model) can be directly used in the experimental analyses and any kind of realistic observable can then be studied both at the theoretical and experimental (detector) level, within the same framework. Second, since the computation of the matrix element is automatic, virtually any process can be simulated at tree level accuracy, opening up the possibility of straightforward experimental analyses of potentially interesting ideas.

The purpose of this work is to present the first step in this direction, i.e., an algorithm for the automatic matrix element generation of amplitudes involving the production (or the decay) of a short-distance quarkonium state with arbitrary spin, angular momentum, and color quantum numbers. The algorithm has been implemented in the matrix element generator MadGraph [12]. Inclusion of the matrix elements into the automatic phase space integrator and event generator MadEvent [13, 14] is ongoing and will be presented in a second publication. The plan of the paper is as follows. In Section 2 we describe the approach followed to project open quark-antiquark amplitudes into those for a given  $2S+1 L_J^{[1,8]}$  state and the validation performed. In Section 3 we present three applications to collider phenomenology. We draw our conclusions in the final section.

## 2. Quarkonium amplitudes in NRQCD

In the framework of Non Relativistic QCD, the cross section associated to a heavy quarkonium production process can be factorized as

$$\sigma(ij \rightarrow \mathcal{Q} + X) = \sum_n \hat{\sigma}(ij \rightarrow Q\bar{Q}(n) + X) \langle \mathcal{O}^{\mathcal{Q}}(n) \rangle, \quad (2.1)$$

where

- $\hat{\sigma}(ij \rightarrow Q\bar{Q}(n) + X)$  is the short distance cross section,
- $\langle \mathcal{O}^{\mathcal{Q}}(n) \rangle$  is the long distance matrix element.

The short distance cross section  $\hat{\sigma}(ij \rightarrow Q\bar{Q}(n) + X)$  is related to the creation of a heavy quark pair in a quantum state  $n$  and it can be computed within perturbation theory, by expanding the amplitude in powers of  $\alpha_S$  and  $v$ , i.e., the strong coupling constant and the relative velocity  $v$ . The sum over  $n$  in Eq. (2.1) *a priori* runs over all possible non-perturbative transitions  $Q\bar{Q}(n) \rightarrow \mathcal{Q}$  and goes therefore beyond the color-singlet approximation, where only the perturbative state with the same quantum numbers as the physical state is included. In particular, the intermediate  $Q\bar{Q}$  state can be in a color-octet, the color being neutralized at later times.

In practice, any quarkonium squared amplitude is obtained by means of an expansion in powers of the relative velocity  $v$  between the heavy quarks. At leading order in  $v$ , the intermediate  $Q\bar{Q}$  state can be specified by the spectroscopic notation

$$n = {}^{2S+1}L_J^{[c]}, \quad (2.2)$$

where  $S$  identifies the spin state of the heavy quark pair,  $L$  the orbital momentum state,  $J$  the total angular momentum state, and  $c = 1, 8$  the color state.

To evaluate the short distance coefficients we use the general algorithms for Feynman diagrams based computations available in MadGraph [12]. MadGraph can provide partonic helicity amplitudes for any process in the Standard Model and beyond at the tree level. In the case of quarkonium, we start from the helicity amplitude information for the open quark-antiquark production and then apply several projection subroutines that select the specific quantum state numbers,  ${}^{2S+1}L_J^{[c]}$ . The projectors are universal and depend only on the quantum numbers to be selected and not on the specific process requested. In fact, only the color projection has to be performed within MadGraph itself since it changes the way the amplitudes are calculated (and in particular selects which diagrams contribute) while spin projections and velocity expansions are performed at runtime. Our method entails that any squared matrix amplitude  $|\mathcal{M}(ij \rightarrow Q\bar{Q}({}^{2S+1}L_J^{[c]}) + X)|^2$  can be generated in any of the models available in MadGraph. Limitations are typical to Feynman-diagram based matrix element generators and are connected to the factorial growth in the number of diagrams. Let us stress a few important points. First, our implementation also allows the calculation of the relativistic corrections for S-wave state production. Second, the employed projectors are general enough to handle the case where the quark and the anti-quark are of different flavor, and therefore have a different mass. In our approach spin

correlation between the quarkonium angular momentum and its decay products are fully included and therefore the information on the quarkonium polarization is kept. In Section 2.3, we discuss two methods to disentangle the longitudinal and transverse parts of the cross section for the transition  $Q\bar{Q}(^3S_1^{[1]}) \rightarrow \mathcal{Q}(J^{PC} = 1^{--})$ .

## 2.1 Projection method and its implementation

In this section, we discuss how to combine the open-quark helicity amplitudes generated by MadGraph in order to select a specific configuration  $^{2S+1}L_J^{[c]}$  for the heavy-quark pair. Our method can be seen as a generalization and automatization of that proposed in Refs. [15, 16].

First we address the computation of the color factors. In MadGraph, the color structure of the parton-level amplitude is obtained by organizing the amplitude into gauge invariant subsets, corresponding to different color flows in the large- $N_C$  limit [17]. The total amplitude is then expressed as a sum over the color flows

$$\mathcal{M} = \sum_m f_m(a, b, \dots) A_m, \quad (2.3)$$

where the  $f_m$ 's are color factors (orthogonal in the large  $N_c$  limit) that depend on color indices  $a, b, \dots$  carried by gluons and quarks, and the  $A_m$ 's are gauge invariant quantities, the so-called partial amplitudes. These amplitudes are computed in MadGraph with the help of HELAS subroutines [18]. The color factors are evaluated at the level of the squared amplitude, each color index being contracted:

$$|\mathcal{M}|^2 = (A_1^*, A_2^*, \dots) \begin{pmatrix} f_1^* f_1 & f_1^* f_2 & \dots \\ f_2^* f_1 & f_2^* f_2 & \dots \\ \vdots & \vdots & \ddots \end{pmatrix} \begin{pmatrix} A_1 \\ A_2 \\ \vdots \end{pmatrix}. \quad (2.4)$$

In MadGraph, the decomposition of the partonic amplitude into partial gauge-invariant amplitudes, as well as the evaluation of the matrix of color factors, are computed automatically for any process at tree-level.

In order to compute the color structure related to the process  $ij \rightarrow Q\bar{Q}(^{2S+1}L_J^{[c]}) + X$ , the quark and anti-quark are required to be in a given color state  $[c]$ . Given that  $3 \otimes \bar{3} = 1 \oplus 8$  the pair can be either in a singlet or octet state that can be obtained by using the projectors [19]

$$\mathcal{C}_1 = \frac{\delta_{ij}}{\sqrt{N_C}}, \quad \mathcal{C}_8 = \sqrt{2}(T^a)_{ij}, \quad (2.5)$$

where  $i$  and  $j$  are the color indices of the heavy quarks. These projectors have been implemented into MadGraph. The color structure for the quarkonium production amplitude is then computed using the same technique as for the open quark production.

Next we consider the projection of the amplitude onto a definite total spin state of the heavy quark pair. The spin projectors were first derived in Ref. [20], and we employ the normalization of Ref. [19]. Since the code is also designed for the production of heavy

quarkonia of mixed flavours, we distinguish the mass of the quark ( $m_1$ ) from that of the anti-quark ( $m_2$ ).  $p_1$  ( $p_2$ ), the momentum of the heavy quark (anti-quark) can be expressed in terms of the total momentum  $P$  and the relative momentum  $p$ :

$$p_1 = \frac{m_1}{m_1 + m_2}P + p, \quad p_2 = \frac{m_2}{m_1 + m_2}P - p. \quad (2.6)$$

The partial helicity amplitudes can be combined to yield a specific spin state for the heavy quark pair:

$$\mathcal{M}(ij \rightarrow Q\bar{Q}(S, \lambda) + X) = \sum_{\lambda_1, \lambda_2} N(\lambda|\lambda_1, \lambda_2) \mathcal{M}(ij \rightarrow Q(\lambda_1)\bar{Q}(\lambda_2) + X), \quad (2.7)$$

where the Clebsch-Gordan coefficients  $N(\lambda|\lambda_1, \lambda_2)$  can be written in terms of the heavy quark spinors<sup>1</sup>,

$$N(\lambda|\lambda_1, \lambda_2) = \frac{1}{\sqrt{8m_1m_2}} \bar{v}(p_2, \lambda_2) \Gamma_S u(p_1, \lambda_1), \quad (2.8)$$

with  $\Gamma_{S=1} = \epsilon_\mu^\lambda \gamma^\mu$  for a spin-one  $Q\bar{Q}$  state ( $\epsilon_\mu^\lambda$  being the polarization vector), and  $\Gamma_{S=0} = \gamma_5$  for a spin-zero  $Q\bar{Q}$  state. Note that this expression is accurate only at leading order in the relative momentum  $p$ . The helicity amplitudes  $\mathcal{M}(ij \rightarrow Q(\lambda_1)\bar{Q}(\lambda_2) + X)$  are computed by MadGraph in a specific Dirac representation employed in the HELAS subroutines [18]. These subroutines can also be invoked for the evaluation of the current in the rhs of Eq. (2.8). The spin projection formula in Eq. (2.7) can then be easily incorporated in a generic numerical algorithm.

We then consider the projection onto a specific orbital state. For  $S$ -wave state production at leading order in  $v$ , one can simply set  $p = 0$  in the short distance amplitude. For  $P$ -wave state, the leading order contribution in  $v$  is given by the derivative of the amplitude with respect to the relative momentum. We approach this derivative numerically by the quotient

$$\frac{\mathcal{M}(\Delta p^i) - \mathcal{M}(0)}{\Delta p^i} \quad (2.9)$$

in the quarkonium rest frame<sup>2</sup>.

Eventually, for spin-one  $P$ -wave states, the spin index is combined with the orbital index in order to select a given angular momentum state,  $J = 0, 1$  or  $2$ .

## 2.2 Relativistic correction to $S$ -wave state production

To evaluate the relativistic corrections to  $S$ -wave state production, the relative momentum  $p$  must be kept different from zero in the amplitude. In this case, we need an expression of the spin projectors accurate to all orders in  $p$ . According to the result of Ref. [21], the Clebsch-Gordan coefficients can be written as

$$N(\lambda|\lambda_1, \lambda_2) = \frac{1}{\sqrt{2}(E + m)} \bar{v}(p_2, \lambda_2) \frac{\not{P} + 2E}{4E} \Gamma_S u(p_1, \lambda_1), \quad (2.10)$$

---

<sup>1</sup>We use the normalization  $\bar{u}(p_i, \lambda_i)u(p_i, \lambda_i) = 2m_i = -\bar{v}(p_i, \lambda_i)v(p_i, \lambda_i)$ .

<sup>2</sup>Wherever we consider a non-zero relative momentum, we replace  $m_i$  by  $E_i$  (the energy of the quark  $i$ ) in Eq. (2.6) in order to enforce the mass-shell condition for the heavy quarks.

where  $E = \frac{\sqrt{P^2}}{2}$ . In this case we assume that the quark and the anti-quark are of the same flavour ( $m_1 = m_2 = m$ ). The contribution to an  $S$ -wave configuration is selected by projecting the amplitude onto the spherical harmonic  $Y_{l=0}^{m=0}$ . This amounts to averaging the amplitude over the direction of the relative momentum. The short distance amplitude is then expanded in powers of  $\frac{p^2}{m^2}$ , each term in the expansion being associated with an independent non-perturbative long distance matrix element.

It has been shown recently that the relativistic corrections arising from the wave function for  $S$ -wave state can be resummed to all orders in  $v$  [22, 23]. Thanks to the following relation among the long distance matrix elements

$$\frac{\langle 0 | \chi^\dagger \kappa (-\nabla^2)^n \psi | \mathcal{Q} \rangle}{\langle 0 | \chi^\dagger \kappa \psi | \mathcal{Q} \rangle} = \left( \frac{\langle 0 | \chi^\dagger \kappa (-\nabla^2) \psi | \mathcal{Q} \rangle}{\langle 0 | \chi^\dagger \kappa \psi | \mathcal{Q} \rangle} \right)^n, \quad (2.11)$$

where  $\kappa$  is either 1 for spin-zero  $Q\bar{Q}$  states or the Pauli matrix  $\boldsymbol{\sigma}$  for spin-one  $Q\bar{Q}$  states, the cross section can be expressed in term of one long distance matrix element:

$$\sigma = \hat{\sigma}(< \mathbf{q}^2 >) \langle 0 | \chi^\dagger \kappa \psi | \mathcal{Q} \rangle \langle \mathcal{Q} | \psi^\dagger \kappa \chi | 0 \rangle, \quad (2.12)$$

where the short distance coefficient has been evaluated at the relative momentum

$$< \mathbf{q}^2 > = \frac{\langle 0 | \chi^\dagger \kappa (-\nabla^2) \psi | \mathcal{Q} \rangle}{\langle 0 | \chi^\dagger \kappa \psi | \mathcal{Q} \rangle}. \quad (2.13)$$

The inclusion of the relativistic corrections arising from the wave function has been implemented in the code, using Eq. (2.12).

### 2.3 Polarization of vector-like quarkonium states

The polarization of vector-like quarkonium states is an interesting exclusive quantity that can provide further information on the production mechanism since it can be measured accurately at colliders. On the theoretical side, the transverse and longitudinal parts of the cross section can be disentangled by using the explicit basis of polarization vectors  $(\varepsilon_L, \varepsilon_{T1}, \varepsilon_{T2})$ , defined by the equations

$$\varepsilon_i \cdot \varepsilon_j = -\delta_{ij}, \quad \varepsilon_i \cdot \mathbf{P} = 0, \quad \varepsilon_L \cdot \mathbf{P} = 0. \quad (2.14)$$

This representation is obviously Lorentz-frame dependent. Usually, the three-vector  $\mathbf{P}$  is evaluated in the lab frame in Eq. (2.14) but other useful frames exist [24].

At hadron colliders a  $^3S_1$  quarkonium state is observed through its decay into leptons. The polarization of the quarkonium can indeed be determined by analyzing the angular distribution of the leptons. Defining  $\theta$  as the angle between the  $\ell^+$  direction in the quarkonium rest frame and the quarkonium direction in the laboratory frame, the normalized angular distribution  $I(\cos \theta)$  is

$$I(\cos \theta) = \frac{3}{2(\alpha + 3)} (1 + \alpha \cos^2 \theta), \quad (2.15)$$

where the relation between  $\alpha$  and the polarization state of the quarkonium is

$$\alpha = \frac{\sigma_T - 2\sigma_L}{\sigma_T + 2\sigma_L}. \quad (2.16)$$

In fact, a more general way to correctly account for the polarization information is to decay the vector-like quarkonium state into leptons at the matrix element level. This can be achieved by replacing the polarization vector of the quarkonium by the leptonic current

$$\frac{\sqrt{3}}{8m\sqrt{\pi}}\bar{u}_{\ell-}(k_1, \lambda_1)\gamma_\mu v_{\ell+}(k_2, \lambda_2). \quad (2.17)$$

and has been set up as an option in our code. Once the vector-like quarkonium decay is required by the user, events are generated that include the information on the lepton momenta too. This method has two main advantages. First it is directly connected to the experimental analysis. The acceptance of the detector may affect the relation between the measured value of the parameter  $\alpha$  and the perturbative polarized cross sections  $\sigma_T$ ,  $\sigma_L$ . However, even when cuts are applied, the angular distribution of the leptons is the physical observable that can be used to compare theory and measurements. Second, it is Lorentz invariant and therefore does not impose an a priori choice for the frame where the polarization information is extracted.

## 2.4 Validation and examples

### 2.4.1 Preliminary checks

In order to gain confidence in our implementation, we have performed several checks listed below.

- Gauge invariance has been systematically verified for all the processes considered by using longitudinal polarization for the external photons or gluons.
- Numerical cancellation among diagrams has been checked for amplitudes that vanish by symmetry considerations:

$$\begin{aligned} A(^1S_0^{[1]} + (2k+1) \text{ photons}) &= 0, \\ A(^3S_1^{[1]} + 2k \text{ photons}) &= 0, \\ A(^1P_1^{[1]} + 2k \text{ photons}) &= 0, \\ A(^3P_1^{[1]} + 2k \text{ photons}) &= 0, \\ A(^3P_{0,2}^{[1]} + (2k+1) \text{ photons}) &= 0, \end{aligned}$$

with  $k = 1, 2, 3$ .

- We have compared our numerical amplitudes against the analytic results point-by-point in phase space for  $(i, j, k = \text{quarks or gluons})$ :
  1.  $ij \rightarrow Qk$  for all  $S$ - and  $P$ -wave states, both color-singlet and color-octet amplitudes, [20][25][26];
  2.  $ij \rightarrow QV$ , with  $V = Z, W$  for the relevant  $S$ - and  $P$ -wave states, both color-singlet and color-octet amplitudes [27];
  3.  $ij \rightarrow Q\phi$ ,  $\phi$  being a scalar or pseudo-scalar for the relevant  $S$ - and  $P$ -wave states, both color-singlet and color-octet amplitudes [28];



(fb)	$^1S_0^{[1]}$	$^3S_1^{[1]}$	$^1P_1^{[1]}$	$^3P_0^{[1]}$	$^3P_1^{[1]}$	$^3P_2^{[1]}$
$e^+e^-@m_Z$	$1.69 \cdot 10^3$	$2.37 \cdot 10^3$	$1.78 \cdot 10^2$	$1.08 \cdot 10^2$	$2.23 \cdot 10^2$	$2.40 \cdot 10^2$
$\gamma\gamma@LEP\ II$	0.519	5.23	0.162	$2.69 \cdot 10^{-2}$	$5.80 \cdot 10^{-2}$	0.266
$\gamma p@HERA$	$3.66 \cdot 10^2$	$1.76 \cdot 10^3$	85.4	21.7	51.7	$2.02 \cdot 10^2$
$pp@LHC$	$gg$	$3.94 \cdot 10^7$	$9.83 \cdot 10^7$	$5.20 \cdot 10^6$	$1.82 \cdot 10^6$	$4.40 \cdot 10^6$
	$q\bar{q}$	$1.37 \cdot 10^5$	$8.34 \cdot 10^5$	$2.95 \cdot 10^4$	$1.10 \cdot 10^4$	$2.69 \cdot 10^4$
$p\bar{p}@Tev\ II$	$gg$	$2.56 \cdot 10^6$	$6.30 \cdot 10^6$	$3.28 \cdot 10^5$	$1.24 \cdot 10^5$	$2.83 \cdot 10^5$
	$q\bar{q}$	$2.64 \cdot 10^4$	$1.62 \cdot 10^5$	$5.70 \cdot 10^3$	$2.12 \cdot 10^3$	$5.21 \cdot 10^3$

**Table 1:** Cross sections (femtobarn) for the color-singlet contributions to the inclusive production of  $B_c$ .

(fb)	$^1S_0^{[8]}$	$^3S_1^{[8]}$	$^1P_1^{[8]}$	$^3P_0^{[8]}$	$^3P_1^{[8]}$	$^3P_2^{[8]}$
$e^+e^-@m_Z$	1.59	2.22	0.167	0.102	0.209	0.225
$\gamma\gamma@LEP\ II$	$4.87 \cdot 10^{-4}$	$4.90 \cdot 10^{-3}$	$1.52 \cdot 10^{-4}$	$2.52 \cdot 10^{-5}$	$5.44 \cdot 10^{-5}$	$2.49 \cdot 10^{-4}$
$\gamma p@HERA$	1.18	8.46	0.506	$7.64 \cdot 10^{-2}$	0.244	1.61
$pp@LHC$	$gg$	$4.11 \cdot 10^5$	$1.79 \cdot 10^6$	$1.17 \cdot 10^5$	$1.38 \cdot 10^4$	$6.23 \cdot 10^4$
	$q\bar{q}$	$1.03 \cdot 10^3$	$7.03 \cdot 10^3$	251	30.7	174
$p\bar{p}@Tev\ II$	$gg$	$2.85 \cdot 10^4$	$1.26 \cdot 10^5$	$8.13 \cdot 10^3$	$9.80 \cdot 10^2$	$4.25 \cdot 10^3$
	$q\bar{q}$	199	$1.37 \cdot 10^3$	48.6	5.95	33.7

**Table 2:** Cross sections (femtobarn) for the color-octet contributions to the inclusive production of  $B_c$ .

The agreement for  $S$  wave amplitudes is at the machine precision, while for  $P$ -waves, which are obtained through a numerical derivative, it is typically at the  $10^{-5}$  level.

#### 2.4.2 Example 1: $B_c$ production at various colliders

$B_c$  production has been extensively studied at various colliders and the many available results provide us with a further testing ground for our code.

We present the results for inclusive cross sections at several colliders for all the  $S$  and  $P$ , both color-singlet and color-octet, states. Since our purpose is to provide reference numbers, we use a very simple set of input parameters common to all processes:

- $m_b = 4.9\text{ GeV}$ ,  $m_c = 1.5\text{ GeV}$ ,  $m_{B_c} = 6.4\text{ GeV}$
- $\langle O \left( ^{2S+1}S_J^{[1]} \right) \rangle = (2J+1) 0.736\text{ GeV}^3$
- $\langle O \left( ^{2S+1}P_J^{[1]} \right) \rangle = (2J+1) 0.287\text{ GeV}^5$
- $\langle O^{[8]} \rangle = 0.01 \langle O^{[1]} \rangle$
- $\mu_{epa} = \mu_F = \mu_R = 12.8\text{ GeV}$

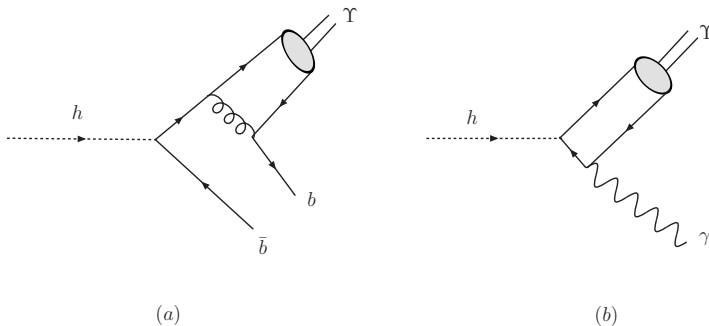


**Figure 1:** Higgs decays into  $\Upsilon$ : in association with a  $b\bar{b}$  pair (a) and with a photon (b).

- $\alpha_S(\mu_R) = 0.189$
- pdf set: cteq6l1
- $\alpha_{EM} = \frac{1}{137}$

Our results are summarized in Tables 1 and 2. For the processes  $gg \rightarrow B_c b\bar{c}$  we compared with Refs. [29, 30], and found agreement for all intermediate states. For color-singlet  $S$ -wave state production in  $\gamma g$  interaction, our results agree with those of Ref. [31]. However, some of the results in the table are new.

#### 2.4.3 Example 2: Higgs decay into $\Upsilon + X$ .

In this section we illustrate through a very simple example how a multi-purpose matrix element code allows to quickly assess the phenomenological relevance of new ideas.

A light Higgs of  $m_H \lesssim 140$  GeV in the Standard Model as well as in extensions such as in SUSY or in generic 2HDM, decays predominantly into  $b\bar{b}$ . Assuming a  $2 \rightarrow 1$  production mechanism at hadron colliders, such  $gg$  or  $b\bar{b}$  fusion, a two  $b$ -jet signature is obtained. Such events are extremely difficult to trigger on and to select from the enormous QCD two-jet background. In fact, in this mass range, the golden channel for discovery is  $H \rightarrow \gamma\gamma$  which has a branching ratio of the order of only  $10^{-3}$  in the SM but has a very clean signature: it can be triggered on and the invariant mass determination is very accurate, giving the possibility of reconstructing a small BW peak over a very large background. However, in some BSM scenarios, such as for example at large  $\tan\beta$  in SUSY or in a generic 2HDM, the branching ratio to two photons is highly suppressed and other decay modes need to be considered.

The presence of a  $\Upsilon$  in the final state could help both in the triggering (through the  $\mu^+\mu^-$  pair) and the invariant mass reconstruction and give a viable discovery mode. Let us consider two cases. As the simplest decay mode, consider  $H \rightarrow \Upsilon b\bar{b}$ , Fig 1 (left). This is analogous to  $Z \rightarrow \Upsilon b\bar{b}$ , which can also be described by the fragmentation function approach. The exact matrix element calculation gives:

$$\frac{\Gamma(H \rightarrow \Upsilon b\bar{b})}{\Gamma(H \rightarrow b\bar{b})} = 1.56 \cdot 10^{-5}, \quad (2.18)$$

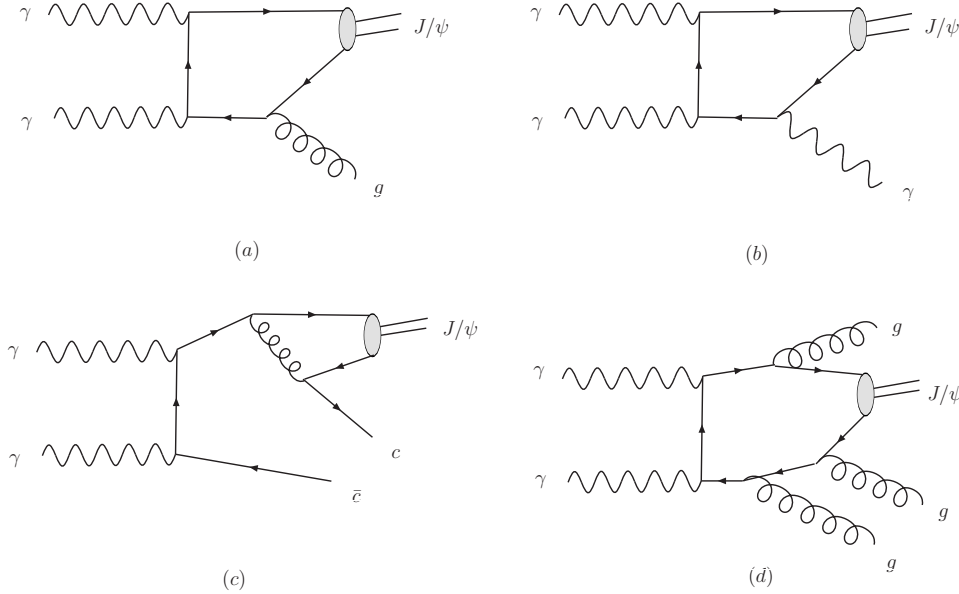


**Figure 2:**  $J/\psi$  direct photoproduction. Production mechanism (a) proceeds via a  $^3S_1^{[8]}$  state, while the photon associated (b), the  $c\bar{c}$  associated and the multi-gluon (d) mechanisms can proceed via a color-singlet transition.

where we used  $m_H = 120$  GeV,  $\langle O_T(^3S_1^{[1]}) \rangle = 9.28$  GeV<sup>3</sup> and  $\alpha_S = 0.118$ .

Another, potentially cleaner mode, which could allow for an excellent invariant mass resolution, is the decay  $H \rightarrow \Upsilon\gamma$ , Fig 1 (right) Note that the crossed decay  $\Upsilon \rightarrow \gamma H$  has been considered before in the literature [32, 33, 34, 35] as a search mode for a light scalar or pseudoscalar and it is known at the NLO accuracy [36]. A straightforward calculation gives:

$$\frac{\Gamma(H \rightarrow \Upsilon\gamma)}{\Gamma(H \rightarrow b\bar{b})} = 6.17 \cdot 10^{-7}, \quad (2.19)$$

where we used  $m_H = 120$  GeV,  $\langle O_T(^3S_1^{[1]}) \rangle = 9.28$  GeV<sup>3</sup> and  $\alpha_{EM} = 1/137$ .

The BR's for both decay modes in the SM (and also in SUSY, since possible large  $\tan\beta$  enhancements cancel in the ratio of the widths), are found to be rather small, also considering that the branching ratio of the quarkonium state into leptons has yet to be included.

### 3. Applications

#### 3.1 $\gamma\gamma \rightarrow J/\psi + X$ at LEP II

$J/\psi$  production in  $\gamma\gamma$  collisions at LEP II ( $\sqrt{S} = 196$  GeV) has been studied in Ref [37]. In that paper, the direct ( $\gamma\gamma$ ), the single resolved ( $\gamma g$ ) and the double resolved ( $gg$ ) components have been taken into account. However, the only direct contribution that

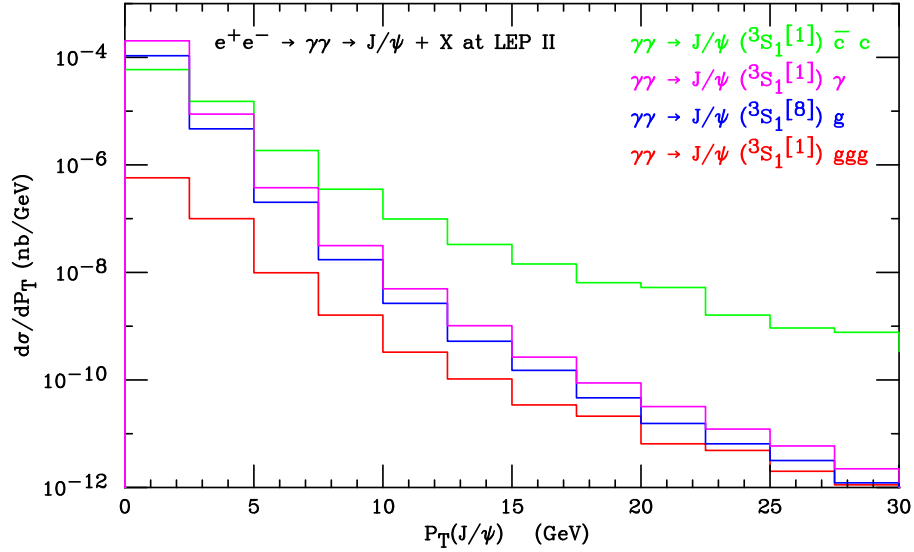


**Figure 3:** Transverse momentum distributions for  $J/\psi$  production in  $\gamma\gamma$  collisions

has been considered is the color-octet transition

$$\gamma\gamma \rightarrow c\bar{c} \left( {}^3S_1^{[8]} \right) g. \quad (3.1)$$

We now address the evaluation of the color-singlet  $J/\psi$  production in (unresolved)  $\gamma\gamma$  interactions. Due to color conservation, the final states  $c\bar{c} \left( {}^3S_1^{[1]} \right) g$  is forbidden. But if we turn the gluon into a photon, the corresponding  $\alpha_{EM}^3$ -process is allowed. Charge conjugation conservation forbids the final state  $c\bar{c} \left( {}^3S_1^{[1]} \right) gg$ . So the only color-singlet process at  $\alpha_{EM}^2\alpha_S^2$  is the associated production. Finally, the channel  $J/\psi +$  light partons occurs at order  $\alpha_{EM}^2\alpha_S^3$ . So the Born-level contributions for the color-singlet production are given by

$$\gamma\gamma \rightarrow c\bar{c} \left( {}^3S_1^{[1]} \right) \gamma, \quad \gamma\gamma \rightarrow c\bar{c} \left( {}^3S_1^{[1]} \right) c\bar{c}, \quad \gamma\gamma \rightarrow c\bar{c} \left( {}^3S_1^{[1]} \right) ggg. \quad (3.2)$$

Note also that the final state  $c\bar{c} \left( {}^3S_1^{[1]} \right) gq\bar{q}$  is also allowed, but is not finite: the fragmentation part  $\gamma \rightarrow q\bar{q} \rightarrow g$  is effectively included in the single-resolved contributions.

Using the Weizsäcker-Williams approximation at LEP2,  $\alpha_S = 0.189$ ,  $m_{J/\psi} = 2m_c = 3$  GeV,  $\alpha_{EM} = 1/137$ ,  $\langle O \left( {}^3S_1^{[1]} \right) \rangle = 1.16$  GeV<sup>3</sup>,  $\langle O \left( {}^3S_1^{[8]} \right) \rangle = 1.06 \cdot 10^{-2}$  GeV<sup>3</sup>, we obtain the  $P_T$  spectra displayed in Fig. 3 for the color-singlet and color-octet processes. We find that the associated  $c\bar{c}$  production is by far the dominant one for  $p_T(J/\psi) > 5$  GeV.

### 3.2 $e^+e^- \rightarrow \eta_c + X$ at $\sqrt{s} = 10.6$ GeV

The production of an  $\eta_c$  state from  $e^+e^-$  collisions has been studied in the context of associated production [38]. Using the inputs  $\alpha_S = 0.26$ ,  $\alpha_{EM} = \frac{1}{137}$ ,  $\langle O \left( {}^1S_0^{[1]} \right) \rangle = 0.387$  GeV<sup>3</sup>, we obtain

$$\sigma(e^+e^- \rightarrow \eta_c + c\bar{c}) = 58.7 \text{ fb}, \quad (3.3)$$

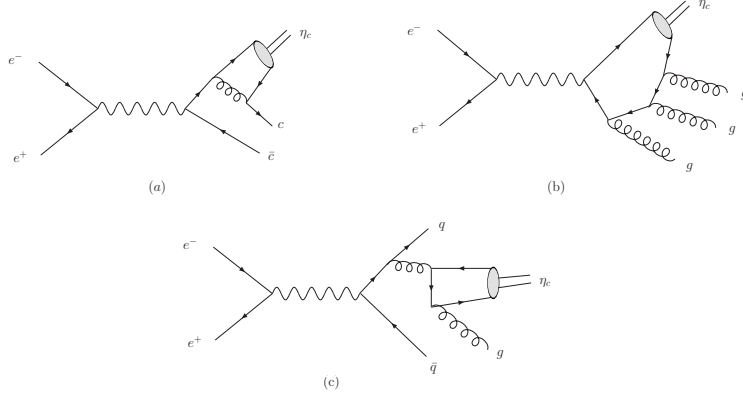


**Figure 4:** Representative diagrams for  $\eta_c$  electroproduction via color-singlet transition: at order  $\alpha_S^2$  in association with a  $c\bar{c}$  pair (a), and at order  $\alpha_S^3$  with three gluons (b) and with a light quark pair (c).

in agreement with the result obtained in Ref. [38].

The contribution to  $\eta_c$  production coming from the associated production with light partons has not been studied so far. The reason is that for color-singlet production, neglecting the exchange of an off-shell  $Z$ , there is no such processes at order  $\alpha_{EM}^2\alpha_S^2$ , due to color and charge conjugation conservation. However, at order  $\alpha_{EM}^2\alpha_S^3$  the following processes can occur:

$$e^+e^- \rightarrow \eta_c ggg, \quad e^+e^- \rightarrow \eta_c q\bar{q}g, \quad (3.4)$$

which are finite and could give a non-negligible cross section due to the larger phase space available. This calculation is straightforward. The code generates the matrix elements for the subprocesses in (3.4), whereas an analytical computation would have been cumbersome. Using a very simple phase-space generator, we checked that the channel  $\eta_c$  + light partons constitutes approximately 10% of the inclusive cross section. The plot in Fig. 5 displays the differential cross section with respect to  $z = \frac{2|\mathbf{P}_{\eta_c}|}{\sqrt{s}}$ , the fraction of momentum taken by the  $\eta_c$ . The total cross sections are given by

$$\sigma(e^+e^- \rightarrow \eta_c ggg) = 3.72 \text{ fb}, \quad \sigma(e^+e^- \rightarrow \eta_c q\bar{q}g) = 1.63 \text{ fb} \quad (3.5)$$

As a result, the associated production is dominating the  $\eta_c$  production

$$\frac{\sigma(e^+e^- \rightarrow \eta_c c\bar{c})}{\sigma(e^+e^- \rightarrow \eta_c X)} = 91.6\% \quad (3.6)$$

It is interesting to note that the corresponding predictions for  $J/\psi$  production are quite different. A similar calculation gives:

$$\sigma(e^+e^- \rightarrow J/\psi c\bar{c}) = 148 \text{ fb}, \quad \sigma(e^+e^- \rightarrow J/\psi gg) = 266 \text{ fb}, \quad (3.7)$$

and therefore, at leading order,

$$\frac{\sigma(e^+e^- \rightarrow J/\psi c\bar{c})}{\sigma(e^+e^- \rightarrow J/\psi X)} = 35.7\%. \quad (3.8)$$

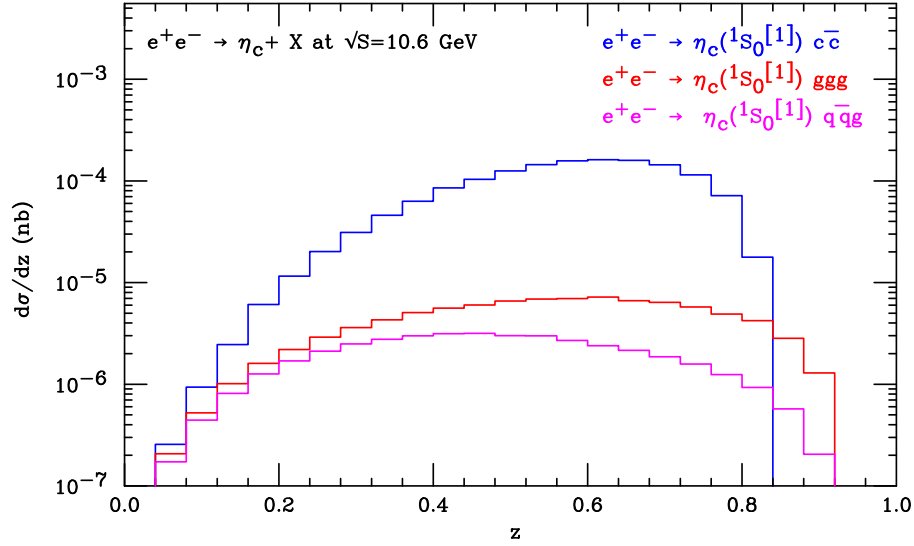


**Figure 5:** Momentum fraction of an  $\eta_c$  in  $e^+e^-$  collisions at  $\sqrt{s} = 10.6$  GeV.

In contrast to the above LO estimate, data indicate that  $J/\psi$  is produced in association with charm most of the time [39]:

$$\frac{\sigma(e^+e^- \rightarrow J/\psi c\bar{c})}{\sigma(e^+e^- \rightarrow J/\psi X)}|_{EXP} = 82 \pm 0.15 \pm 0.14\%. \quad (3.9)$$

It would be interesting to have the analogous measurement for the  $\eta_c$  too.

### 3.3 $p\bar{p} \rightarrow \Upsilon + X$ at the Tevatron

As a last application of our code, we consider the contributions coming from higher order processes to the inclusive production of a  $\Upsilon(^3S_1^{[1]})$  at the Tevatron. In particular, we focus on the prediction for  $p_T$  distribution.

It is easy to verify that the partonic differential cross section at LO, Fig. 6(a), falls off very quickly with the  $p_T$ , as  $1/p_T^8$ , due to the presence of two very off-shell heavy quark propagators in all contributing diagrams. At NLO  $^3S_1^{[1]}$  production in association with gluons features diagrams with only one off-shell heavy quark whose contribution scale as  $1/p_T^6$ , Fig. 6(b). At NNLO both fragmentation contributions, Fig. 6(c), and high-energy enhanced contributions, Fig. 6(d), appear. While a full NNLO calculation including virtual contributions is beyond our present technical capabilities, one can argue that the terms with a different scaling, such as  $1/p_T^6$  and  $1/p_T^4$  appear at the first time at tree-level at order  $\alpha_S^4$  and  $\alpha_S^5$  respectively, and therefore they are finite and are not affected by the (missing) virtual contributions taking place at the same order.<sup>3</sup> Even at tree-level, the calculation of multi-parton amplitudes is very challenging and an automatized computational method is mandatory. For instance, the amplitude for  $gg \rightarrow ^3S_1^{[1]} + 3g$  involves thousands of Feynman diagrams which reduce to several hundreds when the color and spin

<sup>3</sup>This approach can be explicitly validated for the  $1/p_T^6$  terms using the full NLO calculation [8]. A detailed phenomenological analysis is in progress [40].

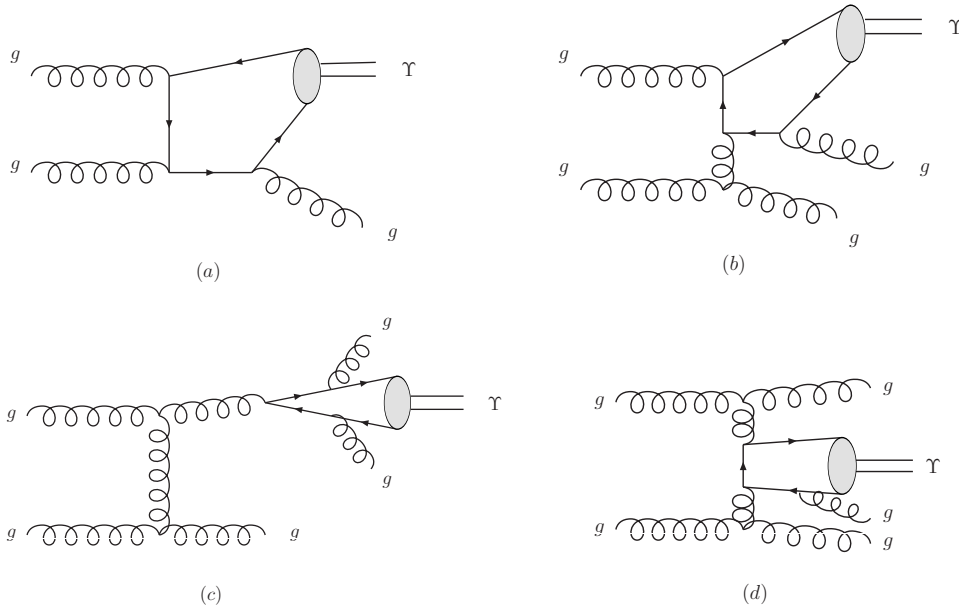


**Figure 6:** Tree-level contributions to  $\Upsilon$  hadroproduction via a color-singlet transition (a) at LO  $\alpha_S^3$ , (b) at NLO  $\alpha_S^4$ , (c,d) at NNLO  $\alpha_S^5$ .

projections are applied. Another complication comes from the large number of different parton-parton subprocesses, whose bookkeeping becomes quite cumbersome for large multiplicities. The above difficulties are easily solved by MadGraph. The identification of the relevant *parton parton*  $\rightarrow {}^3S_1^{[1]} + 3 \text{ partons}$  subprocesses and the generation of the corresponding amplitudes is matter of a few seconds. In Fig. 7 we show the different scaling in  $p_T$  for the various gluonic amplitudes  $gg \rightarrow {}^3S_1^{[1]} + ng$ , with  $n = 1, 2, 3$ . A minimal invariant mass for any gluon (initial or final state) pairs,  $s_{ij} > 4m_b^2$ , is required to avoid the phase space regions where the matrix element is singular. The  $p_T$  shapes, however, depends weakly on the cutoff.

#### 4. Conclusions and Outlook

Quarkonium physics is a rich and active field of research, where our understanding of QCD can be challenged and tested. Collider data, in particular, suggests that our present description of the quarkonium production mechanism is not fully satisfactory yet. Given the importance that  $\Upsilon$  and  $J/\psi$  production will have at the LHC not only as calibration tools, but also for bottom and even top physics, it is mandatory to improve the reliability and the flexibility of our predictions. In this work we have completed the first step towards the development of a multi-purpose Monte Carlo generator for quarkonium physics, i.e., a code for the automatic evaluation of any tree-level matrix element involving a heavy-quark pair in a definite spin and color state. To illustrate its possibilities we have presented several applications to collider physics phenomenology.

The following step will be to interface the matrix element generator to MadEvent for the automatic phase space integration and event generation. With such a code, events at

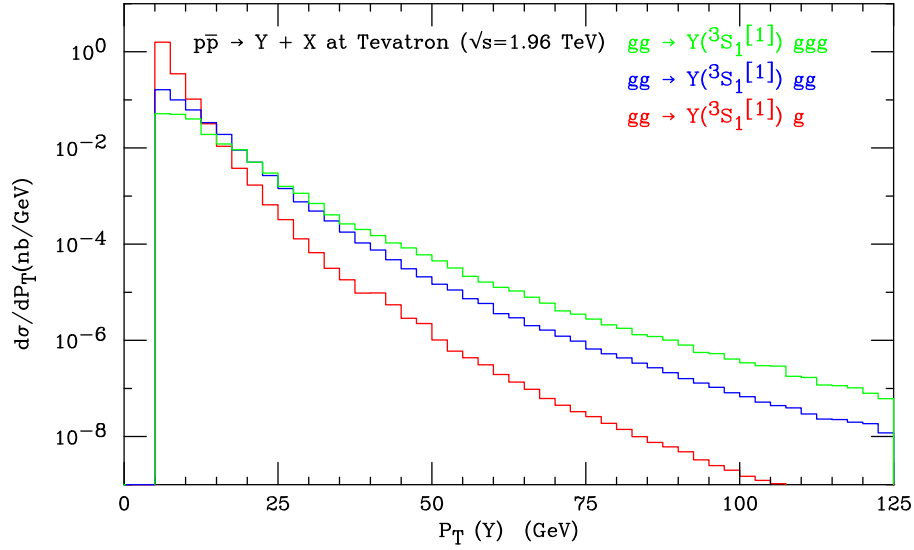


**Figure 7:** Transverse momentum distribution for  $\Upsilon$  production at the Tevatron, Run II. A cut on the minimal invariant mass of each pair of initial and final state gluons,  $s_{ij} > 4m_b^2$ , is applied to avoid soft and collinear divergences. Only amplitudes involving gluons are included. Factorization and renormalization scales are fixed to  $\mu_F = \mu_R = 2m_b$ , with  $m_b = 4.75$  GeV,  $\langle \mathcal{O}(Y) \rangle = 9.28$  GeV<sup>3</sup>. The PDF set is CTEQ6M and  $\alpha_S(2m_b) = 0.180$ .

the parton-level for any process of interest can be generated and then passed through Pythia or Herwig for the parton shower and hadronization and finally to detector simulation. This will allow not only a much wider range of possible studies, such as for example pattern of extra radiation in quarkonium events, but also more direct flow of information from theory to experiment in testing new ideas or new approaches (such as different scaling rules for the various non-perturbative matrix elements). Work in this direction is in progress.

## Acknowledgments

We are thankful to Geoff Bodwin and Eric Braaten for many useful discussions. We would also like to thank all members of CP3 for the great atmosphere and environment that foster our efforts. This work is partially supported by the US National Science Foundation (Contract number NSF PHY 04-26272), by the Belgian Federal Science Policy (IAP 6/11). P.A. is Research Fellow of the Fonds National de la Recherche Scientifique, Belgium.

## References

- [1] N. Brambilla *et al.*, *Heavy quarkonium physics*, [hep-ph/0412158](#).
- [2] G. T. Bodwin, E. Braaten, and G. P. Lepage, *Rigorous QCD analysis of inclusive annihilation and production of heavy quarkonium*, *Phys. Rev.* **D51** (1995) 1125–1171, [[hep-ph/9407339](#)].
- [3] M. Kramer, *Quarkonium production at high-energy colliders*, *Prog. Part. Nucl. Phys.* **47** (2001) 141–201, [[hep-ph/0106120](#)].



- [4] F. Maltoni *et al.*, *Analysis of charmonium production at fixed-target experiments in the NRQCD approach*, *Phys. Lett.* **B638** (2006) 202–208, [[hep-ph/0601203](#)].
- [5] CDF Collaboration, A. Abulencia *et al.*, *Polarization of  $J/\psi$  and  $\psi_{2S}$  mesons produced in  $p\bar{p}$  collisions at  $\sqrt{s} = 1.96$  TeV*, [arXiv:0704.0638](#) [[hep-ex](#)].
- [6] M. Klasen, B. A. Kniehl, L. N. Mihaila, and M. Steinhauser,  *$J/\psi$  plus prompt-photon associated production in two-photon collisions at next-to-leading order*, *Phys. Rev.* **D71** (2005) 014016, [[hep-ph/0408280](#)].
- [7] M. Kramer, *QCD corrections to inelastic  $J/\psi$  photoproduction*, *Nucl. Phys.* **B459** (1996) 3–50, [[hep-ph/9508409](#)].
- [8] J. Campbell, F. Maltoni, and F. Tramontano, *QCD corrections to  $J/\psi$  and  $\Upsilon$  production at hadron colliders*, *Phys. Rev. Lett.* **98** (2007) 252002, [[hep-ph/0703113](#)].
- [9] Y.-J. Zhang and K.-T. Chao, *Double charm production  $e^+e^- \rightarrow J/\psi + c\bar{c}$  at B factories with next-to-leading order QCD correction*, *Phys. Rev. Lett.* **98** (2007) 092003, [[hep-ph/0611086](#)].
- [10] T. Sjostrand, S. Mrenna, and P. Skands, *PYTHIA 6.4 physics and manual*, *JHEP* **05** (2006) 026, [[hep-ph/0603175](#)].
- [11] G. Corcella *et al.*, *HERWIG 6.5 release note*, [hep-ph/0210213](#).
- [12] T. Stelzer and W. F. Long, *Automatic generation of tree level helicity amplitudes*, *Comput. Phys. Commun.* **81** (1994) 357–371, [[hep-ph/9401258](#)].
- [13] F. Maltoni and T. Stelzer, *MadEvent: Automatic event generation with MadGraph*, *JHEP* **02** (2003) 027, [[hep-ph/0208156](#)].
- [14] J. Alwall *et al.*, *MadGraph/MadEvent v4: The New Web Generation*, *JHEP* **09** (2007) 028, [[arXiv:0706.2334](#)] [[hep-ph](#)].
- [15] K. Hagiwara, E. Kou, Z. H. Lin, C. F. Qiao, and G. H. Zhu, *Inclusive  $J/\psi$  productions at  $e^+e^-$  colliders*, *Phys. Rev.* **D70** (2004) 034013, [[hep-ph/0401246](#)].
- [16] P. Artoisenet, J. P. Lansberg, and F. Maltoni, *Hadroproduction of  $J/\psi$  and  $\Upsilon$  in association with a heavy-quark pair*, *Phys. Lett.* **653** (2007) 60, [[hep-ph/0703129](#)].
- [17] F. Maltoni, K. Paul, T. Stelzer, and S. Willenbrock, *Color-flow decomposition of QCD amplitudes*, *Phys. Rev.* **D67** (2003) 014026, [[hep-ph/0209271](#)].
- [18] H. Murayama, I. Watanabe, and K. Hagiwara, *HELAS: Helicity amplitude subroutines for feynman diagram evaluations*, . KEK-91-11.
- [19] A. Petrelli, M. Cacciari, M. Greco, F. Maltoni, and M. L. Mangano, *NLO production and decay of quarkonium*, *Nucl. Phys.* **B514** (1998) 245–309, [[hep-ph/9707223](#)].
- [20] E. L. Berger and D. L. Jones, *Inelastic photoproduction of  $J/\psi$  and  $\Upsilon$  by gluons*, *Phys. Rev.* **D23** (1981) 1521–1530.
- [21] G. T. Bodwin and A. Petrelli, *Order  $v^4$  corrections to S-wave quarkonium decay*, *Phys. Rev.* **D66** (2002) 094011, [[hep-ph/0205210](#)].
- [22] G. T. Bodwin, D. Kang, T. Kim, J. Lee, and C. Yu, *Relativistic corrections to  $e^+e^- \rightarrow J/\psi + \eta_c$  in a potential model*, *AIP Conf. Proc.* **892** (2007) 315–317, [[hep-ph/0611002](#)].

- [23] G. T. Bodwin, D. Kang, and J. Lee, *Potential-model calculation of an order- $v^2$  NRQCD matrix element*, *Phys. Rev.* **D74** (2006) 014014, [[hep-ph/0603186](#)].
- [24] M. Beneke, M. Kramer, and M. Vanttinen, *Inelastic photoproduction of polarised  $J/\psi$* , *Phys. Rev.* **D57** (1998) 4258–4274, [[hep-ph/9709376](#)].
- [25] P. L. Cho and A. K. Leibovich, *Color-octet quarkonia production II*, *Phys. Rev.* **D53** (1996) 6203–6217, [[hep-ph/9511315](#)].
- [26] P. L. Cho and A. K. Leibovich, *Color octet quarkonia production*, *Phys. Rev.* **D53** (1996) 150–162, [[hep-ph/9505329](#)].
- [27] B. A. Kniehl, C. P. Palisoc, and L. Zwirner, *Associated production of heavy quarkonia and electroweak bosons at present and future colliders*, *Phys. Rev.* **D66** (2002) 114002, [[hep-ph/0208104](#)].
- [28] B. A. Kniehl, C. P. Palisoc, and L. Zwirner, *Associated production of bottomonia and higgs bosons at hadron colliders*, *Phys. Rev.* **D69** (2004) 115005, [[hep-ph/0404039](#)].
- [29] C. H. Chang, C. Driouichi, P. Eerola, and X. G. Wu, *Bcveppy: An event generator for hadronic production of the  $B_c$  meson*, *Comput. Phys. Commun.* **159** (2004) 192, [[hep-ph/0309120](#)].
- [30] C. H. Chang, J. X. Wang, and X. G. Wu, *Bcveppy2.0: A upgrade version of the generator bcveppy with an addendum about hadroproduction of the P-wave  $B_c$  states*, *Comput. Phys. Commun.* **174** (2006) 241, [[hep-ph/0504017](#)].
- [31] A. V. Berezhnoy, V. V. Kiselev, and A. K. Likhoded, *Non-abelian nature of asymmetry in the production of  $B_c$  mesons in gluon photon interactions*, *Phys. Atom. Nucl.* **61** (1998) 252–259, [[hep-ph/9710429](#)].
- [32] B. McElrath, *Invisible quarkonium decays as a sensitive probe of dark matter*, *Phys. Rev.* **D72** (2005) 103508, [[hep-ph/0506151](#)].
- [33] M. L. Mangano and P. Nason, *Radiative quarkonium decays and the NMSSM Higgs interpretation of the hyperCP  $\Sigma^+ \rightarrow p\mu^+\mu^-$  events*, *Mod. Phys. Lett. A* **22** (2007) 1373, [[hep-ph/0704.1719](#)].
- [34] B. McElrath, *Light higgses and dark matter at bottom and charm factories*, [arXiv:0712.0016](#) [[hep-ph](#)].
- [35] M.-A. Sanchis-Lozano, *A light non-standard higgs boson: to be or not to be at a (super)  $b$  factory?*, [arXiv:0709.3647](#) [[hep-ph](#)].
- [36] P. Nason, *QCD radiative corrections to  $\Upsilon$  decay into scalar  $+\gamma$  and pseudoscalar  $+\gamma$* , *Phys.Lett.B* **175** (1986) 223.
- [37] M. Klasen, B. A. Kniehl, L. N. Mihaila, and M. Steinhauser, *Evidence for colour-octet mechanism from CERN LEP2  $\gamma\gamma \rightarrow J/\psi + X$  data*, *Phys. Rev. Lett.* **89** (2002) 032001, [[hep-ph/0112259](#)].
- [38] K.-Y. Liu, Z.-G. He, and K.-T. Chao, *Inclusive charmonium production via double  $c\bar{c}$  in  $e^+e^-$  annihilation*, *Phys. Rev.* **D69** (2004) 094027, [[hep-ph/0301218](#)].
- [39] Belle Collaboration, K. Abe *et al.*, *Study of double charmonium production in  $e^+e^-$  annihilation at  $\sqrt{s} \approx 10.6$  GeV*, *Phys. Rev.* **D70** (2004) 071102, [[hep-ex/0407009](#)].
- [40] P. Artoisenet, J. Campbell, J.-P. Lansberg, F. Maltoni, and F. Tramontano, “in progress.”.